U.S. DEPARTMENT OF THE INTERIOR
U.S. GEOLOGICAL SURVEY

Prepared for the
NATIONAL AERONAUTICS AND SPACE ADMINISTRATION

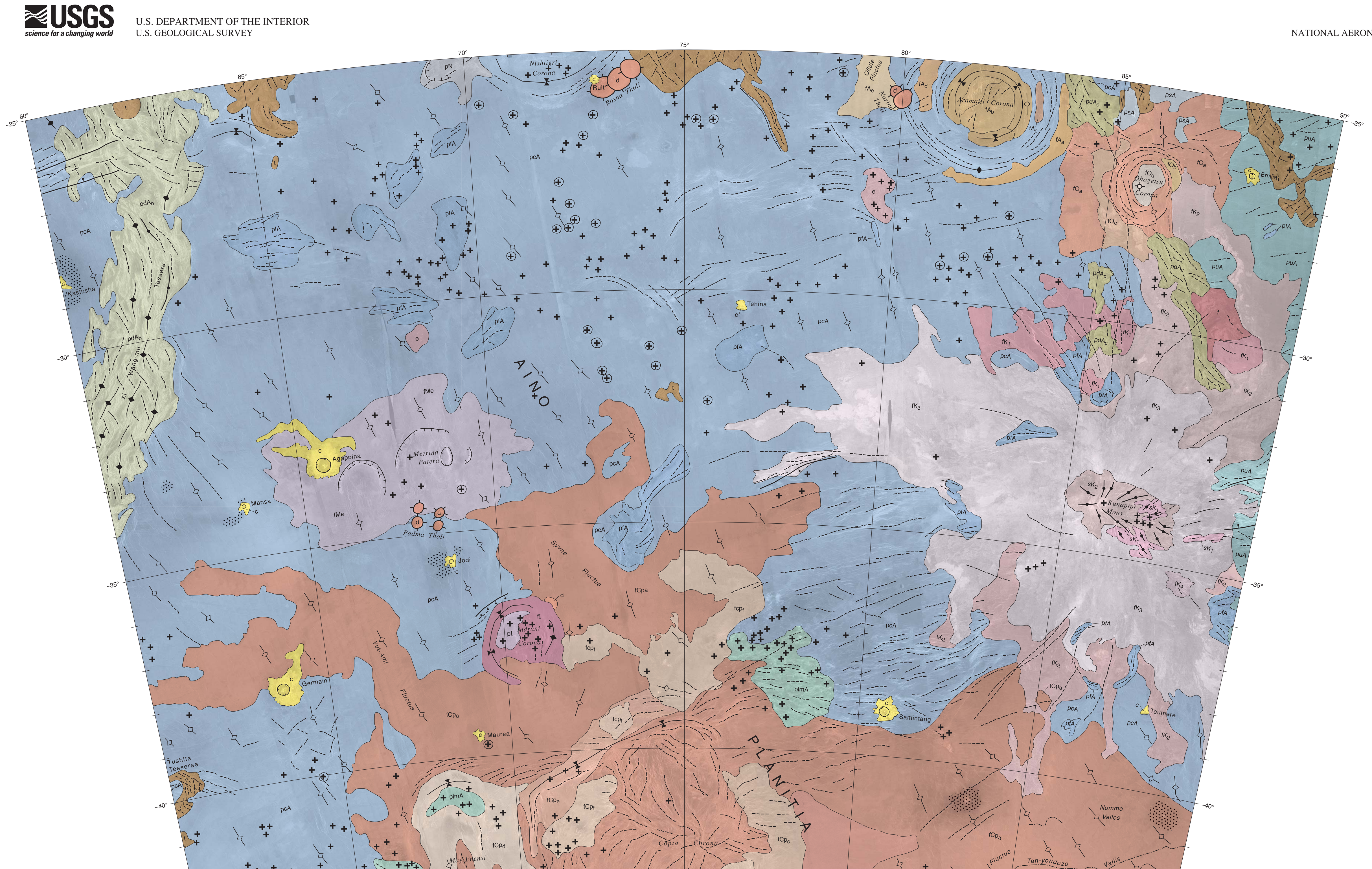

SCALE 1:4 711 886 (1 mm = 4.712 km) AT –25° LATITUDE
1:5 000 000 AT –34° and –73° LATITUDES
LAMBERT PROJECTION

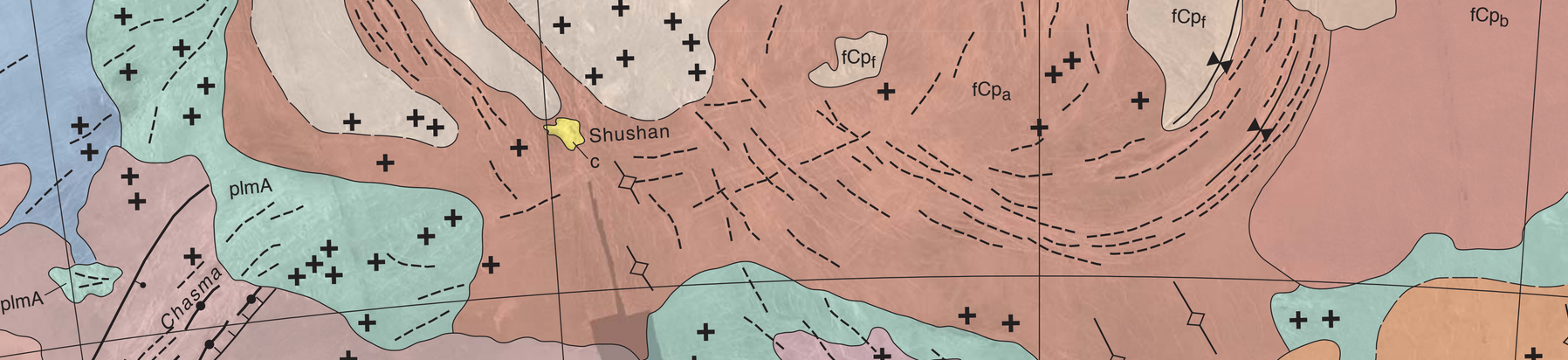

INTERIOR—GEOLOGICAL SURVEY, RESTON, VA—2003
Prepared on behalf of the Planetary Geology and Geophysics Program, Solar System Exploration Division, Office of Space Science, National Aeronautics and Space Administration
Edited by Derrick D. Hirsch; cartography by Darlene A. Ryan and Beatrice C. Landavazo
Manuscript approved for publication November 8, 2002

CORRELATION OF MAP UNITS

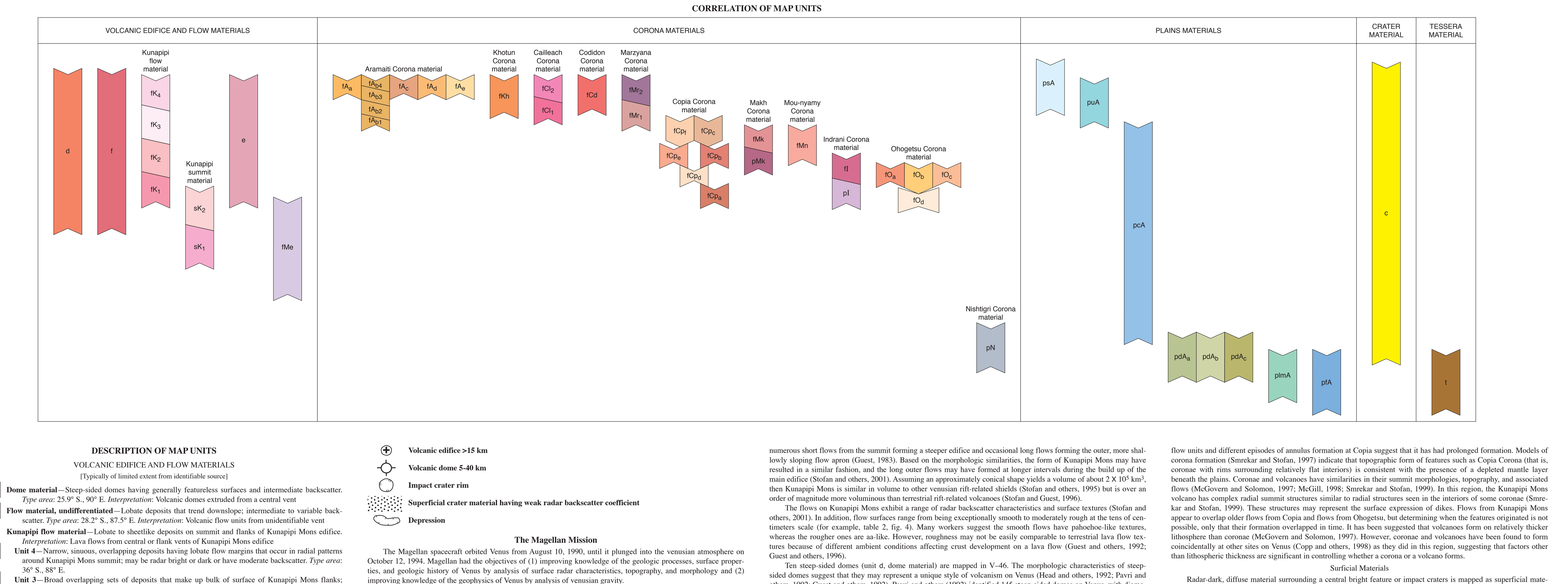

DESCRIPTION OF MAP UNITS

VOLCANIC EDIFICE AND FLOW MATERIALS

[Typically of limited extent from identifiable source]

d **Dome material**—Steep-sided domes having generally featureless surfaces and intermediate backscatter. *Type area*: 25.9° S., 90° E. *Interpretation*: Volcanic domes extruded from a central vent

f **Flow material, undifferentiated**—Lobate deposits that trend downslope; intermediate to variable backscatter. *Type area*: 28.2° S., 87.5° E. *Interpretation*: Volcanic flow units from unidentifiable vent

Kunapipi flow material—Lobate to sheetlike deposits on summit and flanks of Kunapipi Mons edifice. *Interpretation*: Lava flows from central or flank vents of Kunapipi Mons edifice

fK_4 **Unit 4**—Narrow, sinuous, overlapping deposits having lobate flow margins that occur in radial patterns around Kunapipi Mons summit; may be radar bright or dark or have moderate backscatter. *Type area*: 36° S., 88° E.

fK_3 **Unit 3**—Broad overlapping sets of deposits that make up bulk of surface of Kunapipi Mons flanks; tends to have moderate to dark appearance in radar; superposed by unit 4 of Kunapipi flow material. *Type area*: 35° S., 85° E.

fK_2 **Unit 2**—Digitate overlapping sets of deposits on outer flanks of Kunapipi Mons; tends to have moderate to dark appearance in radar. *Type area*: 31° S., 87° E.

fK_1 **Unit 1**—Digitate deposits on outer flanks of Kunapipi Mons; tends to have moderate to dark appearance in radar; superposed by unit 2 of Kunapipi flow material. *Type area*: 31° S., 84° E.

Kunapipi summit material—Plains materials cut by fractures at Kunapipi Mons summit. *Interpretation*: Volcanic materials from Kunapipi Mons edifice that have been deformed by extensional fractures interpreted to be surface expression of dikes

sK_2 **Unit 2**—Plains material at summit of Kunapipi Mons edifice; has radar-bright lineaments trending approximately radial to summit, with numerous pits. *Type area*: 33.75° S., 86.1° E.

sK_1 **Unit 1**—Similar to unit 2 of Kunapipi summit material; both units are embayed by unit fK_3. *Type area*: 33.8° S., 87.2° E.

e **Edifice field material**—Numerous small shields and cones surrounded by lobate deposits having moderate backscatter. Multiple occurrences in map area with varying superposition relationships. *Type area*: 29.5° S., 69° E. *Interpretation*: Volcanic edifice fields of varying ages

fMe **Mezrina Patera flow material**—Mottled sheetlike and digitate deposits surrounding four calderas. Superposes unit pcA. *Type area*: 34° S., 69.5° E. *Interpretation*: Volcanic center having three remnant calderas and one complete caldera, with flows of four centers not distinguishable

CORONA MATERIALS

[Material related to coronae, typically of limited extent and varying from deformed materials to digitate or sheetlike deposits]

Aramaiti Corona flow material—Sheetlike to digitate deposits interior to and surrounding Aramaiti Corona. *Interpretation*: Lava units formed from vents within or at margins of Aramaiti Corona, largely postdating formation of corona topography and deformation

fA_e **Unit E**—Broad deposits extending from margins of Aramaiti Corona. *Type area*: 27° S., 79° E.

fA_d **Unit D**—Sheetlike deposits having moderate to dark radar backscatter cross section and lobate flow margins. *Type area*: 26° S., 81° E.

fA_c **Unit C**—Similar to unit D of Aramaiti Corona flow material. *Type area*: 26.5° S., 83.1° E.

fA_b **Unit B**—Set of superimposed units (1–4) having lobate margins and moderate to dark radar backscatter cross section; deformed by arcuate fractures. *Type area*: 26° S., 82.5° E.

fA_a **Unit A**—Deposits having moderate to dark radar backscatter cross section and lobate flow margins. *Type area*: 27° S., 83.5° E.

fKh **Khotun Corona flow material**—Sheetlike deposits having moderate, mottled radar backscatter cross section. Contains northeast-trending wrinkle ridges and has lobate flow margins. *Type area*: 48° S., 80° E. *Interpretation*: Extensive sheets of lava from vents within or at margins of Khotun Corona

Cailleach Corona flow material—Sheetlike deposits having lobate margins. *Interpretation*: Lava units formed from vents within or at margin of Cailleach Corona

fCl_2 **Unit 2**—Sheetlike deposits having moderate radar backscatter cross section and lobate flow margins; cut by northwest-trending wrinkle ridges. *Type area*: 48.75° S., 88° E.

fCl_1 **Unit 1**—Deposits having moderate to dark radar backscatter cross section and arcuate fractures; embayed by unit 2 of Cailleach Corona flow material. *Type area*: 47.1° S., 88° E.

fCd **Codidon Corona flow material**—Mottled sheetlike deposits having moderate radar backscatter cross section and lobate flow margins that surround corona in V–45 quadrangle. *Type area*: 45° S., 60.1° E. *Interpretation*: Extensive sheets of lava from vents within or at margin of Codidon Corona

Marzyana Corona flow material—Sheetlike deposits extending from Marzyana Corona. *Interpretation*: Extensive sheets of lava from vents within or at margin of Marzyana Corona. Multiple stages of emplacement indicated

fMr_2 **Unit 2**—Moderate to bright radar backscatter cross section; cut by northeast-trending fractures. *Type area*: 48.5° S., 70° E.

fMr_1 **Unit 1**—Sheetlike deposits having moderate to dark radar backscatter cross section and lobate flow margins that surround Marzyana Corona in V–57 quadrangle. *Type area*: 46° S., 70° E.

Copia Corona flow material—Lobate and sheetlike deposits associated with Copia Corona. *Interpretation*: Units composed of extensive sheets of lava from vents within and (or) at margins of Copia Corona. Multiple stages of emplacement indicated

fCp_f **Unit F**—Lobate deposits having numerous small edifices, northwest-trending wrinkle ridges, corona-related deformation, and moderate radar backscatter cross section. *Type area*: 41.5° S., 72° E.

fCp_e **Unit E**—Lobate deposits having east-trending fractures. *Type area*: 41.2° S., 71° E.

fCp_d **Unit D**—Lobate deposits having small edifices, corona-related deformation, and dark to mottled radar backscatter cross section. *Type area*: 42.2° S., 69.5° E.

fCp_c **Unit C**—Lobate deposits having numerous small edifices, corona-related fractures, and moderate radar backscatter cross section. *Type area*: 41.5° S., 77.5° E.

fCp_b **Unit B**—Featureless sheetlike deposits having moderate radar-backscatter cross section. *Type area*: 43° S., 79.5° E.

fCp_a **Unit A**—Sheetlike deposits having moderate radar backscatter cross section and lobate flow margins. Cut by extensive corona-related deformation, northwest-trending ridges, and numerous small edifices. *Type area*: 39.15° S., 70° E.

pMk **Makh Corona material, undifferentiated**—Plains materials extensively deformed by radial and concentric deformation of Makh Corona. Numerous small edifices. *Type area*: 48° S., 84.5° E. *Interpretation*: Early Makh Corona flow material or previously existing plains unit deformed and uplifted by formation of Makh Corona

fMk **Makh Corona flow material**—Sheetlike deposits having mottled to dark radar backscatter cross section and lobate flow margins. *Type area*: 49.25° S., 86.5° E. *Interpretation*: Lava from vents within or at margins of Makh Corona

fMn **Mou-nyamy Corona flow material**—Sheetlike deposits having moderate radar backscatter cross section and lobate flow margins that surround Mou-nyamy Corona in V-45 quadrangle. *Type area*: 45.5° S., 64° E. *Interpretation*: Extensive sheets of lava from vents within or at margin of Mou-nyamy Corona

fI **Indrani Corona flow material**—Sheetlike deposits having mottled radar backscatter cross section, multiple small edifices, and lobate flow margins. *Type area*: 37.75° S., 69.3° E. *Interpretation*: Extensive sheets of lava from vents within and (or) at margins of Indrani Corona

pI **Indrani Corona plains material**—Plains material cut by multiple sets of fractures. Stands higher than surrounding plains and is embayed by Indrani Corona flow material (unit fI). *Type area*: 37.25° S., 70.2° E. *Interpretation*: Plains material, possibly early volcanic material from Indrani Corona, that has been uplifted to form part of interior and rim of Indrani Corona

Ohogetsu Corona flow material—Lobate and sheetlike deposits associated with Ohogetsu Corona. *Interpretation*: Lava units from vents within or at margins of Ohogetsu Corona

fO_d **Unit D**—Sheetlike deposits having moderate to mottled radar backscatter cross section and lobate margins; deformed by corona-related fracturing. *Type area*: 27° S., 86.5° E.

fO_c **Unit C**—Digitate, lobate radar bright to dark deposits. *Type area*: 28° S., 85.5° E.

fO_b **Unit B**—Limited, fractured deposit having moderate to dark radar backscatter cross section. *Type area*: 27.5° S., 87° E.

fO_a **Unit A**—Lobate deposits having moderate radar backscatter cross section and numerous small edifices. *Type area*: 28° S., 84° E.

pN **Nishtigri Corona plains material**—Deposits having moderate radar backscatter cross section; deformed; has volcanic edifices. Embayed by Aino composite plains material (unit pcA). *Type area*: 25.2° S., 69.75° E. *Interpretation*: Units probably formed by lava associated with formation of Nishtigri Corona, subsequently uplifted, deformed, and then embayed by Aino composite plains material

PLAINS MATERIALS

[Typically cover large areas and ranges from dark to moderate backscatter cross section]

psA **Aino smooth plains material**—Areally limited deposits having relatively dark radar backscatter cross section, scattered small edifices, and (or) pits. Embays all other plains units with which it is in contact; cut by wrinkle ridges. *Type occurrence*: 43.5° S., 89.5° E. *Interpretation*: Volcanic plains that have undergone little deformation. Occurs in multiple areas, cannot determine age relationship between different outcrops

puA **Aino uniform plains material**—Extensive, generally level deposits having relatively uniform backscatter over hundreds of kilometers; minor occurrences of domes, cones, shields, fractures, and ridges. *Type area*: 46.5° S., 89° E. *Interpretation*: Volcanic plains composed primarily of areally extensive flow units

pcA **Aino composite plains material**—Extensive, generally level deposits having variable backscatter characterized by multiple patch volcanoes, areas of fracturing, wrinkle ridges, domes, cones and shields. *Type area*: 31° S., 66° E. *Interpretation*: Volcanic plains built up of a number of interfingered deposits, with minor extension and compression occurring locally

Aino deformed plains material—Plains material cut by sets of fractures. *Interpretation*: Volcanic plains that have undergone intense localized extension (unit A), or a combination of compression and extension (units B, C)

pdA_c **Unit C**—Plains material cut by ridges and fractures trending northwest. Generally radar bright. *Type area*: 28° S., 87° E.

pdA_b **Unit B**—Plains material cut by a high concentration of fractures and ridges dominantly trending northeast to south-southwest. *Type area*: 30° S., 62° E.

pdA_a **Unit A**—Plains material cut by a high concentration of fractures and grabens trending northeast to southwest; few volcanic edifices. *Type area*: 47° S., 65° E.

plmA **Aino lineated and mottled plains material**—Extensive unit containing numerous small domes, cones and shields, and associated lobate flows; unit exhibits radar-bright, dark and moderate backscatter. Typically contains fractures in multiple orientations. *Type area*: 46° S., 74° E. *Interpretation*: Numerous small volcanic edifices and associated flows forming volcanic plains; cut by subsequent deformation

pfA **Aino fractured plains material**—Limited, heavily fractured deposits, having moderate radar backscatter; typically higher standing and embayed by composite plains unit; single orientation of fractures; absence of small edifices. *Type area*: 31° S., 70° E. *Interpretation*: Volcanic plains that have undergone multiple episodes of deformation

TESSERA MATERIAL

[Highly deformed material that occurs as isolated, unrelated outcrops]

t **Tessera material**—Generally radar bright, locally high standing deposits containing two or more orientations of lineaments; typical occurrences are small and appear to be embayed by plains and flow materials. *Type area*: 25.2° S., 65.25° E. *Interpretation*: Extremely tectonically deformed, locally older materials embayed by younger volcanic plains and flows. Occurrences may contain fractures and ridges

CRATER MATERIAL

[Material related to impact craters]

c **Crater material, undifferentiated**—Radar bright or dark floor, central peak, wall, rim, and ejecta materials. *Type area*: 38.5° S., 274.8° E. *Interpretation*: Deposits and structures formed by hypervelocity impact

Contact—Dashed where approximately located or arbitrarily located based on edifice densities

Wrinkle ridge—Interpreted as compressional deformation analogous to lunar and martian wrinkle ridges

Lineament

Graben—Bar and ball on downthrown side

Normal fault—Bar and ball on downthrown side

Scarp—Line marks top of slope; hachures point downslope

Ridge crest—Large-scale topographic features commonly associated with coronae

Trough—Large-scale topographic features associated with coronae

Channel, narrow and sinuous—Interpreted as formed by lava erosion

Volcanic edifice <15 km

Volcanic edifice >15 km

Volcanic dome 5-40 km

Impact crater rim

Superficial crater material having weak radar backscatter coefficient

Depression

The Magellan Mission

The Magellan spacecraft orbited Venus from August 10, 1990, until it plunged into the venusian atmosphere on October 12, 1994. Magellan had the objectives of (1) improving knowledge of the geologic processes, surface properties, and geologic history of Venus by analysis of surface radar characteristics, topography, and morphology and (2) improving knowledge of the geophysics of Venus by analysis of venusian gravity.

The Magellan spacecraft carried a 12.6-cm radar system to map the surface of Venus. The transmitter and receiver systems were used to collect three datasets: synthetic aperture radar (SAR) images of the surface, passive microwave thermal emission observations, and measurements of the backscattered power at small angles of incidence, which were processed to yield altimetric data. Radar imaging and altimetric and radiometric mapping of the venusian surface were done in mission cycles 1, 2, and 3, from September 1990 until September 1992. Ninety-eight percent of the surface was mapped with radar resolution of approximately 120 meters. The SAR observations were projected to a 75-m nominal horizontal resolution; these full-resolution data compose the image base used in geologic mapping. The primary polarization mode was horizontal-transmit, horizontal-receive (HH), but additional data for selected areas were collected for the vertical polarization sense. Incidence angles varied from about 20° to 45°.

High-resolution Doppler tracking of the spacecraft was done from September 1992 through October 1994 (mission cycles 4, 5, 6). High-resolution gravity observations from about 950 orbits were obtained between September 1992 and May 1993, while Magellan was in an elliptical orbit with a periapsis near 175 kilometers and an apoapsis near 8,000 kilometers. Observations from an additional 1,500 orbits were obtained following orbit-circularization in mid-1993. These data exist as a 75° by 75° harmonic field.

Magellan Radar Data

Radar backscatter power is determined by the morphology of the surface at a broad range of scales and by the intrinsic reflectivity, or dielectric constant, of the material. Topography at scales of several meters and larger can produce quasi-specular echoes, with the strength of the return greatest when the local surface is perpendicular to the incident beam. This type of scattering is most important at very small angles of incidence, because natural surfaces generally have few large tilted facets at high angles. The exception is in areas of steep slopes, such as ridges or rift zones, where favorably tilted terrain can produce very bright signatures in the radar image. For most other areas, diffuse echoes from roughness at scales comparable to the radar wavelength are responsible for variations in the SAR return. In either case, the echo strength is also modulated by the reflectivity of the surface material. The density of the upper few wavelengths of the surface can have a significant effect. Low-density layers, such as crater ejecta or volcanic ash, can absorb the incident energy and produce a lower observed echo. On Venus, a rapid increase in reflectivity exists at a certain critical elevation, above which high-dielectric minerals or coatings are thermodynamically stable. This effect leads to very bright SAR echoes from virtually all areas above that critical elevation.

The measurements of passive thermal emission from Venus, though of much lower spatial resolution than the SAR data, are more sensitive to changes in the dielectric constant of the surface than to roughness. As such, they can be used to augment studies of the surface and to discriminate between roughness and reflectivity effects. Observations of the near-nadir backscatter power, collected using a separate smaller antenna on the spacecraft, were modeled using the Hagfors expression for echoes from gently undulating surfaces to yield estimates of planetary radius, Fresnel reflectivity, and root-mean-square (rms) slope. The topography data produced by this technique have horizontal footprint sizes of about 10 km near periapsis and a vertical resolution of approximately 100 m. The Fresnel reflectivity data provide a comparison to the emissivity maps, and the rms slope parameter is an indicator of the surface tilts, which contribute to the quasi-specular scattering component.

INTRODUCTION

The Aino Planitia quadrangle (V–46) extends from 25°–50° S. latitude, 60°–90° E. longitude. The quadrangle was mapped at 1:5,000,000 scale as part of the NASA Planetary Geologic Mapping Program.

Aino Planitia is a lowland region in the southern hemisphere of Venus and is southwest of Thetis Regio in western Aphrodite Terra. It is dominated by low-lying plains units that are characterized by northeast-trending wrinkle ridges and numerous small volcanic edifices, including shields, domes, and cones. The quadrangle contains a major volcano, Kunapipi Mons, and portions of Juno Chasma (fig. 1). A northern extension of the Lada Terra highland is in the southwestern portion of the map (P, fig. 1). Eight coronae are mapped in the quadrangle (table 1), the largest of which is the 500-km-diameter Copia Corona (fig. 1). The region is dominated by plains that are interpreted to be of volcanic origin. Most of the plains units are composites of flow units of differing ages.

The overall topography of V–46 consists of low-lying plains slightly below Mean Planetary Radius (MPR, 6051.84 km, Ford and Pettengill, 1992) (fig. 2). The summit of Kunapipi Mons is the highest point in the quadrangle, at about 2.2 km above MPR; the lowest points in rifts and troughs are at about 1.7 km below MPR. The regions that are the roughest at Magellan radar wavelengths in the quadrangle occur along the rim of Copia Corona, with most regions being relatively smooth (roughness comparable to the average Venus surface; for example, Campbell and Campbell, 1992) (table 2). Emissivity values in the quadrangle vary from 0.82–0.90 (fig. 3, table 2).

MAPPING TECHNIQUES

Standard planetary geologic mapping techniques (for example, Wilhelms, 1972, 1990) were used to construct a geologic map of the V–46 quadrangle. Magellan synthetic aperture radar (SAR) data were used for the map base; over 90% of the quadrangle is covered by both right- and left-looking data. Synthetic parallax stereo images with a 10_ vertical exaggeration, produced by the U.S. Geological Survey (USGS) at Flagstaff, were used extensively in the determination of the stratigraphic relationships between map units. In particular, embayment relationships could be clearly seen in the synthetic stereo data. Magellan altimetry, root mean square (RMS) slope, reflectivity, and emissivity data sets (Pettengill and others, 1992; Campbell, 1999) provide additional information on the properties of map units.

Utilization of both right- and left-looking data sets was critical in producing the map. Right-looking data were used for the initial map base. Units were then transferred to a left-look map base. This exercise brought out subtle differences between map unit characteristics in the two data sets and also illustrated the pitfalls of mapping with radar data. In places, contacts clearly visible in right-looking data could not be identified in left-looking data, and vice versa. In addition, by chance, four steep-sided domes fall into narrow data gaps in the left-looking mosaic of the quadrangle but could be mapped using right-looking data.

Full-resolution Magellan image mosaics (FMAP's) produced by the U.S. Geological Survey were fundamental to the construction of the geologic map. Unit characters and boundary locations not resolvable at C1-MIDR (Cycle 1, Mosaicked Image Data Record) scale (250 m/pixel) were clearly seen at FMAP scale (75 m/pixel). The large format of the FMAP prints, the synthetic stereo data, and the digital data were key to determining stratigraphic relationships. Apparently, contradictory stratigraphic relationships between major map units were commonly caused by the presence of additional subtle units only noticeable through digital manipulation of FMAP data.

Other difficulties arose in using radar data to construct a geologic map (for example, Ford and others, 1993). Geologic units will only be visible in radar data if they have backscatter characteristics distinctly different from the surrounding units. This situation is not likely always to be the case in plains regions or lava flow fields, where younger and older units of similar backscatter may be mistakenly incorporated into a single unit. If the surface properties of a unit change laterally, potentially its radar signature can also change, and it may be mapped incorrectly as two or more units. In addition, structures tend to be more readily identified if they are oriented perpendicular to the radar look direction (for example, Stofan and others, 1989). Thus, in Magellan data, north-south-trending lineaments will tend to be well defined, but east-west structures are likely to be underrepresented or only weakly represented in the image data unless they have associated rough talus slopes.

GENERAL GEOLOGY

MAPPABLE UNITS

Plains Materials

We have identified six plains material units in the Aino Planitia quadrangle: Aino fractured plains material (unit pfA), Aino lineated and mottled plains material (unit plmA), Aino deformed plains material (unit pdA, with members a–c), Aino composite plains material (unit pcA), Aino uniform plains material (unit puA), and Aino smooth plains material (unit psA). Each of these units comprises many smaller plains units of varying age, which we group together to form a mappable unit. These smaller plains units have been grouped on the basis of their similarity in appearance and stratigraphic position relative to other plains units. Some of the plains units, including pfA and plmA, crop out as isolated patches of materials.

Units pfA, plmA, and pdA are the oldest plains units in the Aino Planitia quadrangle. Because these three older plains units are not in contact with each other, determining their ages relative to one another is not possible. All of the older plains units contain more deformational features than younger plains units, although some younger plains units have been locally intensely deformed. The older plains are all embayed by Aino composite plains material (unit pcA), which in turn is embayed by Aino uniform plains material (unit puA) and Aino smooth plains material (unit psA).

The Aino fractured plains material (unit pfA) contains northeast-, north-, or northwest-trending fractures and (or) grabens that are less than 100 km long and less than 5 km wide. This unit occurs as numerous kipukas throughout V–46 quadrangle; the largest outcrop is at 31° S., 85.5° E. This unit is interpreted to be deformed volcanic plains, although no flow features are identified. The outcrops of this unit are grouped due to general morphologic similarities; though some outcrops of unit pfA may represent fragments of a larger, embayed unit, other outcrops may be unrelated.

The Aino deformed plains material (unit pdA) contains ridges and (or) fractures. Each outcrop of the Aino deformed plains material has a unique set of deformational features, so this material has been subdivided into three units. Unit A (pdA_a), centered at 48° S., 64° E., is dominated by a set of parallel to sub-parallel fractures spaced less than 5 km apart and lying along a slight topographic depression, interpreted to be a rift zone. This rift is embayed by surrounding plains units, unlike an adjacent rift <100 km to the northeast that cuts surrounding plains units. Unit B (pdA_b), centered at 29° S., 62° E., has ridges trending approximately north-south that are cut by later east-west-trending extensional fractures and grabens. Unit C (pdA_c), centered at 29° S., 87° E., has approximately north-south-trending ridges. Units B, C, and D of the Ohogetsu Corona flow material (units fO_b, fO_c, and fO_d, respectively) and flows from Kunapipi Mons (units fK_1 and fK_2) are superposed on unit C of the Aino deformed plains material. Units A–C of the Aino deformed plains material are most likely volcanic in origin and have undergone extensive deformation. These units probably did not form contemporaneously.

The Aino lineated and mottled plains material (unit plmA) contains fractures and (or) grabens arrayed in a variety of orientations. It also crops out in patches and is the third most areally extensive plains unit in this quadrangle. The unit contains numerous small domes, cones, and shields, along with fractures in multiple orientations. Numerous lobate flows associated with the small edifices give the unit a mottled or patchy appearance. In some areas, this unit exhibits a narrowly spaced (5–15 km), northeast-trending wrinkle ridge set. In general, however, the unit is highly fractured, making wrinkle ridges difficult to identify. The Aino lineated and mottled plains material is interpreted to be made up of volcanic flows that have been deformed by several episodes of tectonism, including deformation associated with the formation of wrinkle ridges and grabens. Small volcanoes within unit plmA both predate and postdate deformation, indicating that the development of small volcanoes has persisted over time within this unit.

The most extensive plains unit in Aino Planitia is the Aino composite plains material (unit pcA). This plains material is regional in scale and is interpreted to be dominantly volcanic in origin, as it is composed of numerous overlapping flows. The presence of numerous flows gives the unit a patchy or mottled appearance. The composite plains unit is postdated by most corona-related materials in this region, much of the visible materials associated with Kunapipi Mons, and the Aino uniform (unit puA) and smooth (unit psA) plains materials. Unit pcA has been deformed in places by fracturing associated with Juno Chasma, other east-trending groups of fractures, and wrinkle ridges. Most of unit pcA is characterized by northwest-trending wrinkle ridges. In the northernmost portions of unit pcA, the wrinkle ridges are less developed, and in some areas are absent altogether.

The second largest plains unit in Aino Planitia is the Aino uniform plains material (unit puA). This unit is superposed on the Aino composite plains and continues eastward into the Juno Chasma region (D.A. Senske, oral commun., 2000). This plains material is interpreted to be volcanic in origin based on the identification of diffuse flow fronts within the unit and the unit's lobate boundaries. It consists of more sheetlike flow units than the Aino composite plains unit and is superposed by small patches of radar-dark flows grouped as the Aino smooth plains material (unit psA). Both units puA and psA are crosscut by the same wrinkle ridge sets as unit pcA. Outcrops of units psA and puA occur dominantly in the eastern third of the quadrangle.

In summary, the lowland regions of Aino Planitia can be separated into six mappable plains units. The six plains units that formed during episodes of resurfacing of relatively similar style and scale have occurred over time, interspersed with periods of regional or local extension and compression. A typical 1000 km X 1000 km region within Aino Planitia has numerous identifiable flow units, of which approximately 60% can be tied to a source. The scale of resurfacing of these flow units varies from <100 km^2 to over 50,000 km^2. Smaller volcanic flow units are common, with approximately 40% of the flow units having resurfaced an area of 50–150 km^2.

Volcanic Edifice and Flow Materials

The Aino Planitia quadrangle contains a variety of mappable volcanic landforms, including a major shield volcano (Kunapipi Mons, 34° S., 84° E.), a flow complex associated with Mezrina Patera, steep-sided domes, and small volcanic edifices.

Mezrina Patera (unit fMe) consists of two irregularly shaped calderas <40 km across, lying within a depression centered at 33.3° S., 68.8° E. It is surrounded by both uniform and more digitate flows that were later deformed by wrinkle ridges. Approximately 50 km to the west of Mezrina Patera lies a crescent-shaped embayed ridge, which may represent an earlier buried caldera in this volcanic complex. Mezrina Patera flows (unit fMe) postdate the emplacement of unit pcA but predate flows associated with Copia Corona (unit fCp_a).

Kunapipi Mons is about 2 km high and is built over Juno Chasma, a major rift, and in this respect is similar to several other venusian volcanoes (for example, Gula and Sif Montes) (Stofan and others, 2001). Kunapipi Mons has a central edifice with slopes of a few degrees and a radius of about 240 km. An apron of flows extends beyond the central edifice onto the surrounding terrain to a radial distance of about 700 km. The outer flow apron has slopes generally less than 1°.

The summit of Kunapipi Mons consists of an elongate plateau region, with its long axis oblique to the Juno Chasma rift. Volcanic centers exist at each end of the summit plateau. At the western end is a central edifice with radial summit fractures and associated flow deposits. The eastern center is a cluster of small shields and pits with associated lava on a domical topographic high. Deposits from both centers, unit sK_2, embay unit sK_1, summit deposits that are heavily radially fractured. These and other radial fractures at the summit and on the flanks of Kunapipi Mons are interpreted to be the surface manifestation of dikes (Stofan and others, 2001). The presence of radial fractures in both units sK_1 and sK_2 indicates that multiple episodes of dike intrusion have occurred at the summit of Kunapipi Mons. The summit deposits are embayed by flank material (unit fK_3).

The central edifice of Kunapipi Mons is made up of shorter more numerous flows (units $fK_{3,\ 4}$), compared with the outer apron that consists of fewer more extensive flows (units $fK_{1,\ 2}$). Flank eruptive sites can be identified on the main topographic edifice as well as on the flatter outer apron. In comparison, Mount Etna has a similar profile that results from numerous short flows from the summit forming a steeper edifice and occasional long flows forming the outer, more shallowly sloping flow apron (Guest, 1983). Based on the morphologic similarities, the form of Kunapipi Mons may have resulted in a similar fashion, and the long outer flows may have formed at longer intervals during the build up of the main edifice (Stofan and others, 2001). Assuming an approximately conical shape yields a volume of about 2 X 10^5 km^3, then Kunapipi Mons is similar in volume to other venusian rift-related shields (Stofan and others, 1995) but is over an order of magnitude more voluminous than terrestrial rift-related volcanoes (Stofan and Guest, 1996).

The flows on Kunapipi Mons exhibit a range of radar backscatter characteristics and surface textures (Stofan and others, 2001). In addition, flow surfaces range from being exceptionally smooth to moderately rough at the scale of centimeters scale (for example, table 2, fig. 4). Many workers suggest the smooth flows have pahoehoe-like textures, whereas the rougher ones are aa-like. However, roughness may not be easily comparable to terrestrial lava flow textures because of different ambient conditions affecting crust development on a lava flow (Guest and others, 1992; Guest and others, 1996).

Ten steep-sided domes (unit d, dome material) are mapped in V–46. The morphologic characteristics of steep-sided domes suggest that they may represent a unique style of volcanism on Venus (Head and others, 1992; Pavri and others, 1992; Guest and others, 1992). Pavri and others (1992) identified 145 steep-sided domes on Venus, with diameters ranging from 7 to 94 kilometers and average heights of about 700 m. On the basis of their gross morphology, some workers interpreted steep-sided domes to have a silicic composition (Head and others, 1992; Pavri and others, 1992; McKenzie and others, 1992). However, terrestrial silicic domes are smaller and tend to have extremely rough surfaces with different distributions and types of surface structures, such as raised vent regions and ridged zones (Anderson and others, 1998; Plaut and others, 1994). In addition, compositional determinations are non-unique when based on gross morphologic properties (Fink and Griffiths, 1990; Bridges and Fink, 1992; Guest and others, 1992; Sakimoto and Zuber, 1995; Bridges, 1997; Stofan and others, 2000).

In this quadrangle, steep-sided domes have diameters from about 18 to 45 km. Most occur in three main groups: (1) Padma Tholi centered at 34.7° S., 68.8° E., (2) Rosna Tholi centered at 25.5° S., 73.3° E., and (3) Narina Tholi centered at 25.8° S., 80° E. The latter two groups are superposed on the rims of Nishtigri and Aramaiti Coronae, respectively. The surfaces of the steep-sided domes in V–46 have roughnesses comparable to typical plains units, tend to have few fractures or other lineaments, and contain numerous small pits (Stofan and others, 2000). The fracture patterns on the surfaces of steep-sided domes indicate that the domes deformed, most likely due to cooling or further intrusion of magma, after a stable crust had formed (Stofan and others, 1997, 2000).

Numerous small edifices (diameters <10 km) are found within most of the plains and flow units. At two sites in V–46, groups of these edifices and their deposits are mapped as edifice field material (unit e). At both of these sites, edifice field material is superposed on unit pcA. Edifices within individual units formed over time. Plains or flow units with higher densities of fractures tend to have a greater concentration of small edifices, suggesting that fracturing facilitates edifice formation. Some edifice flows are undeformed, whereas others have been deformed by later fractures or wrinkle ridges.

Lobate deposits trending downslope from a ridge centered at 28.2° S., 87.5° E. are mapped as flow material, undifferentiated (unit f). The deposits have intermediate to variable backscatter and are interpreted to be volcanic flow units from unidentifiable vents. The unit superposes flow units from Kunapipi Mons.

Corona Materials

Eight coronae, ranging in size from 125 to 500 km, are mapped in the V–46 quadrangle (table 1). In addition, flow units associated with three coronae outside the quadrangle—along the southern and western boundaries—are also mapped (units fMr_1 and fMr_2 and units fCd and fMn). All but two of the coronae in this region (Nishtigri and Makh) have mappable associated deposits that are interpreted to be volcanic in origin. Based on the classification scheme of Stofan and others (1992), seven are classified as concentric coronae, and one, Copia, as an asymmetric corona.

Nishtigri Corona has been embayed by the Aino composite plains material (unit pcA). This corona has a discontinuous, partial rim surrounding an inner dome-shaped area. The rim has concentric fractures, as does the slope of the inner dome. Nishtigri Corona plains material (unit pN) may be composed of flow materials associated with Nishtigri or it may be an older uplifted or high-standing plains unit.

Indrani Corona comprises two units: interior plains material (unit pI) and flow material (unit fI). The Indrani Corona plains material overlies a dome-shaped high surrounded by a trough. The Indrani Corona flow material is interpreted to be of volcanic origin. Unit pI may be either uplifted older plains or earlier stage Indrani flow material. Unit fI completely surrounds and embays unit pI; unit fI superposes unit pcA and early-stage Copia flows (unit fCp_a) but is overlain by later Copia flows (unit fCp_f). The annulus of the corona is a topographic ridge made up of unit fI, indicating that deformation postdated volcanism.

Ohogetsu and Copia Coronae are the most geologically and stratigraphically complex coronae in this region. Ohogetsu, a topographic depression, is superposed on a belt of relatively high standing, deformed plains material (unit pdA_c). Analysis of synthetic stereo data supports that the northern half of the corona was uplifted after both annulus formation and flows associated with the corona had formed. One of its flow units (unit fO_d) is superposed on the Aino composite plains material (unit pcA) and the Aino uniform plains material (unit puA), but it is not possible to determine whether the corona began forming before the emplacement of these plains units. Flows from Kunapipi Mons (unit fK_2) superpose Ohogetsu unit fO_b and are superposed by unit fO_c. Flows from Aramaiti Corona (unit fA_a) superpose unit fO_d, indicating that at least some volcanic activity at Aramaiti postdates some flow emplacement at Ohogetsu Corona.

Copia Corona, the largest corona in V–46, has six associated flow units (units $fCp_{a–f}$). The corona has been named as two features, Copia and May-Enensi, but it is a single, complex structure. A raised rim surrounds about 70% of the corona. Most of the interior of Copia is flat, with irregular topography in the northeastern portion of the interior. Copia is surrounded by an annulus that varies in topography and tectonic deformation. To the southeast, an arc-shaped segment of annulus is composed primarily of ridges. The eastern and northeastern portions of the annulus are composed of narrow ridge and trough topography, with closely spaced fractures on the topographic ridge. The northwestern annulus has more widely spaced fractures, which extend across the ridge, the trough, and into the surrounding plains. The western annulus segment consists of a topographic ridge with no apparent associated fracture annulus.

Flow units associated with Copia Corona postdate formation of unit pcA and unit plmA. To the west, the annulus of the corona is composed of a segment of unit plmA, which we interpret to have been partially uplifted before flooding by unit fCp_a. The earliest mappable corona unit (unit fCp_a) is cut by interior deformation within the corona and the annulus to the northwest and southeast. The interior deformation also cuts the annulus to the east, but it is embayed by units fCp_d, fCp_e, and fCp_f. The southeastern annulus also postdates wrinkle ridges to the south. The fCp_b unit embays the annulus to the southeast. This unit is superposed by unit fCp_c, which also embays the southeastern annulus segment. To the north, the annulus is embayed by units fCp_e and fCp_f. We interpret the variations in styles of deformation of the annulus of Copia and its complex stratigraphic relationships with Copia-associated volcanism to indicate that the annulus did not form in a single event.

The interior of Makh Corona is characterized by intensely deformed material (unit pMk). This material may represent earlier flows from Makh or a plains unit that was subsequently deformed. The corona, a circular structure with a topographically raised rim, is centered at 47° S., 85.5° E. It has a radial set of fractures on its southern rim. The interior of the corona is a dome-shaped structure with radial and some concentric fractures. Radial groups of fractures are seen at other coronae on Venus, sometimes in the interior of the corona and sometimes on their annulus (Smrekar and Stofan, 1999). Cailleach Corona consists of an interior flow unit (unit fCl_1) that is superposed by a later flow unit (unit fCl_2). Cailleach is a depression, with no apparent topographic rim. Flows from this corona (fCl_2) are superposed on puA and Makh Corona materials.

Aramaiti Corona is topographically complex, with an outer partially fractured rim surrounding an inner domical high. The inner high and rim are separated by a trough (fig. 3). The outer rim coincides with closely spaced fractures that make up the tectonic annulus. The annulus deforms the local plains (unit pcA). The inner topographic high is covered with a series of flow units (units $fA_{b1–4}$), which overlie unit pcA. Other flows associated with the corona (units fA_a, fA_c, fA_d) also superpose unit pcA, but none of the flow units associated with Aramaiti come into contact with each other, therefore no reliable timing for the volcanism can be established. In several locations, some of the flow units (units fA_a, fA_c, fA_d) embay the annulus.

Khotun Corona consists of a partial topographic rim that surrounds an interior depression. Its interior and surrounding region are composed of extensive sheet flows (unit fKh). The annulus is made up of concentric fractures on the topographic rim. Khotun Corona flows (unit fKh) are superposed on units plmA, fCp_a, pMk, and fMk.

Flow units from Mou-nyamy Corona (unit fMn; 49.5° S., 59° E.; quadrangle V–45), Marzyana Corona (unit fMr; 53° S., 67.5° E.; quadrangle V–57), and Codidon Corona (unit fCd; 46° S., 56° E.; quadrangle V–45) extend into V–46. All of these flows superpose unit pcA. Flows from Codidon Corona (unit fCd) superpose materials from Mou-nyamy (unit fMn). Flows from Marzyana Corona are split into two units of intermediate brightness, with an older flow unit (unit fMr_1) superposing Copia flows, unit plmA, and unit pdA_a. Unit fMr_1 is superposed by younger flows from Marzyana Corona (unit fMr_2) and flows from Mou-nyamy (unit fMn).

Tessera Material

Five outcrops of highly deformed material have been mapped as tessera (unit t). Units with a single or very dominant direction of fractures were mapped as unit pfA or unit pdA, whereas units with two or more dominant fracture and (or) ridge orientations were mapped as unit t, following the convention for Venus (Venus Geologic Mappers Handbook, Tanaka and others, 1994). Tessera material tends to be relatively rough at Magellan radar wavelengths (table 2) and stands higher than the surrounding units. We interpret tessera to represent locally older tectonically deformed regions, usually embayed by younger volcanic plains and flows. The outcrops in this region are too small to determine if the complex deformation was produced in a single event or multiple events, nor can we determine if all of the outcrops formed in the same event. Deformation at these fragments is similar to deformation in the interior of Copia Corona and Makh Corona; some tessera fragments could be inliers of corona materials, as suggested previously by Hansen and Willis (1996). Four tessera outcrops are embayed by plains, corona, or dome materials (units pcA, d, psA, fO_d, puA). One lies in a belt of deformed plains material (unit pdA_a). The tessera material predates the deformed plains material at this one location.

Crater Material

Fourteen impact craters are mapped in the V–46 quadrangle (unit c; table 3). Four have central peaks; nine are at least partially dark floored. The dark material could be ponded impact melt, later flood lavas, or fine debris. Agrippina crater is the only impact crater in this quadrangle that has associated outflow deposits formed by fluidized ejecta (for example, Schaber and others, 1992).

Stratigraphically, eight craters are on the Aino composite plains material (unit pcA) and one is on the Aino uniform plains unit (unit puA). Leila crater (table 3) lies on the boundary between units pcA and puA and is embayed by unit puA. Four craters are on Copia Flow A material (unit fCp_a), and one on unit fMr_2. Agrippina crater lies on the boundary and superposes both units pcA and fMe; Germain crater superposes both units pcA and fCp_a, and Ruit crater superposes both a steep-sided dome and unit pcA.

STRUCTURE

Wrinkle Ridges

Wrinkle ridges are common on plains units throughout Aino Planitia. Wrinkle ridges generally have a northwest–southeast trend within the quadrangle, although their spacing and density varies. They are common on plains units on Venus (Squyres and others, 1992; McGill, 1993) and are thought to result from limited amounts of horizontal compression and shortening (for example, Plescia and Golombek, 1986).

Wrinkle ridges appear on all plains units, including the youngest units psA and puA. In most areas of unit pcA, narrow, northwest–southeast-trending wrinkle ridges are spaced 2–3 km apart. In a few areas, these deformational features are in a polygonal pattern. The closely spaced ridges are also accompanied in some areas by a parallel set of more broadly spaced (20–40 km) wrinkle ridges. These more widely spaced ridges also occur without the more closely spaced ridges. Whether this set is contemporaneous with the finer spaced set is not known.

No wrinkle ridges are observed on Kunapipi Mons flows. Some flow materials associated with coronae have wrinkle ridges; other corona flows have no wrinkle ridges. Most of the corona flows lacking wrinkle ridges cover a relatively small area, except for unit fCp_b, one of the larger flow units associated with Copia. Other Copia units, such as units fCp_f and fCp_a, are deformed by wrinkle ridges. Wrinkle ridges are not present on units in the northeastern corner of the map area. The non-uniform distribution, spacing, and the multiple sets of wrinkle ridges may indicate that the ridges formed due to multiple episodes of horizontal compression.

Fractures and Faults

Aino Planitia is characterized by several sets of fractures, some of which are grabens. Major sets of fractures are near 27° S., 78° E., along Juno Chasma between Kunapipi Mons and Copia Corona, and on the Lada Terra plateau at 48° S., 74° E. Another minor set is to the southwest and southeast of Aramaiti Corona. Most of the fracture sets trend approximately east-west, parallel to the trend of Juno Chasma. The set on the Lada Terra plateau trends northwest and intersects a set trending northeast. The northeast-trending set postdates unit pMk but predates unit fKh.

We interpret the fractures to have resulted from limited horizontal extension, most likely associated with the regional tectonism that produced Juno Chasma. The northwest-trending set on Lada Terra occurs in an older plains unit (unit plmA) and likely results from an earlier episode of extension.

Rifts

Juno Chasma is a major trough system that extends east-west starting at Artemis Corona. It reaches depths of over 1.5 km below mean planetary radius and contains linear fractures interpreted to be normal faults produced by extension and rifting (fig. 1). In the Aino Planitia quadrangle, the rift appears in two segments, separated by Kunapipi Mons. To the east of Kunapipi Mons, Juno Chasma is a well-defined trough approximately 80 km across with a superposed 175-km-wide belt of fracturing (at A, fig. 1). Kunapipi Mons is superposed on the rift. To the southwest of Kunapipi Mons, the trough has no well-defined topographic expression but is manifested as a 350-km-wide zone of fractures and grabens (at B, fig. 1). At the western margin of Copia Corona lies another trough with associated faulting (at C, fig. 1). We interpret these three segments of Juno Chasma to have formed synchronously and to have been subsequently overlain by deposits from Kunapipi Mons. Flows from this large edifice clearly flow down segments of the trough and overlie all faulting. To the southwest of the westernmost segment of Juno Chasma (rift C, fig. 1), lies an older rift. Materials within this older rift (unit pdA_a) are embayed by all surrounding units, unlike the Juno rift. This segment is parallel to the segments of Juno Chasma and may represent an earlier episode of Juno extension.

The formation of Copia Corona has overlapped in time with the formation of Juno Chasma, with flows from the corona superposed on segments of the trough and obscuring some faulting. Later activity resulted in faulting cutting the corona. The formation of the rift segment to the east of Copia also was coeval with Copia Corona. This rift segment breaches the rim of the corona, but flows originating from within the corona are superposed on rift faults.

To the south of Copia Corona lies a plateau, corresponding to the northern margin of Lada Terra. Flows from the corona postdate formation of the plateau, as their emplacement was controlled by plateau topography. The plateau boundary lies along the unit plmA–fKh and plmA–fCp_a contacts and is demarked by a relatively abrupt, 1 km scarp. The plateau region is bounded to the north in this quadrangle by two rifts; older rift materials (pdA_a) and the western extension of Juno Chasma (rift C, fig. 1). The plateau in this region is composed of corona flows and older plains material (unit plmA). We interpret unit plmA, which forms a low ridge at the margin of the plateau, to have been uplifted, as similar outcrops of this material occur at lower elevations proximal to the plateau. Plateau-shaped highlands on Venus are typically characterized by tessera terrain, which also occurs at other sites in Lada Terra. However, this portion of Lada Terra is atypical of plateau highlands on Venus in that it appears to be dominated by plains, similar to the Lakshmi plateau.

Coronae

The coronae in this region exhibit a great variation in morphology. Copia Corona is extremely complex, with six associated volcanic units and extensive deformation. Khotun Corona is relatively simple. The coronae in this quadrangle also vary greatly in topographic expression, from a depression to a rim surrounding an inner dome. The multiple flow units and different episodes of annulus formation at Copia suggest that it has had prolonged formation. Models of corona formation (Smrekar and Stofan, 1997) indicate that topographic form of features such as Copia Corona (that is, coronae with rims surrounding relatively flat interiors) is consistent with the presence of a depleted mantle layer beneath the plains. Coronae and volcanoes have similarities in their summit morphologies, topography, and associated flows (McGovern and Solomon, 1997; McGill, 1998; Smrekar and Stofan, 1999). In this region, the Kunapipi Mons volcano has complex radial summit structures similar to radial structures seen in the interiors of some coronae (Smrekar and Stofan, 1999). These structures may represent the surface expression of dikes. Flows from Kunapipi Mons appear to overlap older flows from Copia and flows from Ohogetsu, but determining when the features originated is not possible, only that their formation overlapped in time. It has been suggested that volcanoes form on relatively thicker lithosphere than coronae (McGovern and Solomon, 1997). However, coronae and volcanoes have been found to form coincidentally at other sites on Venus (Copp and others, 1998) as they did in this region, suggesting that factors other than lithospheric thickness are significant in controlling whether a corona or a volcano forms.

Surficial Materials

Radar-dark, diffuse material surrounding a central bright feature or impact craters is mapped as superficial material (stipple pattern). Four such areas are associated with an impact crater. Four other sites lack a central crater and are similar to other "splotch" features on Venus (for example, Schaber and others, 1992). These features are interpreted to be produced upon the break-up of an impactor in the atmosphere (Phillips and others, 1991). The resulting shock wave pulverizes the upper layers of the surface, producing a roughly circular region of impact debris (Phillips and others, 1991; Zahnle, 1992).

GEOLOGIC HISTORY

As is the case for most of Venus, units that are not adjacent are extremely difficult to correlate in time. The relative randomness of the impact crater population (for example, Schaber and others, 1992; Hauck and others, 1998; Campbell, 1999) makes it virtually impossible to use crater statistics to date individual mapped units. In some cases, a particular set of structures, such as a wrinkle ridge set, can be used to tie distant units together in time. However, most age relationships presented here are local rather than regional. An additional difficulty arises in attempting to relate features that are long-lived. Coronae and large volcanoes have complex histories and are likely to have formed over relatively extended periods (for example, Guest and Stofan, 1997; Copp and others, 1998; Smrekar and Stofan, 1999).

The history of V–46 suggests that plains formation in this region has been a repetitive, incremental process. The oldest units in the Aino Planitia quadrangle were deformed to varying degrees at different times to form highly deformed units (unit t) and less deformed units (units pdA, pfA, plmA). These units are probably, but not conclusively, volcanic in origin. We have no information on how long a period these units represent, and, due to their limited areal extent, little knowledge of their original nature. For example, tessera fragments could have been originally larger fragments of a deformed basement (for example, Ivanov and Head, 1996), or they could represent unrelated episodes of deformation possibly related to corona formation (for example, Hansen and Willis, 1996). Similarly, the oldest plains units (units pdA, pfA, plmA) represent an unknown extent in time and are cut by fractures that probably resulted from different episodes of regional extension. The only two of these units that come into contact are one of the outcrops of deformed terrain mapped as tessera (unit t) and one of the outcrops of deformed plains material (unit pdA_a). In this case, the tessera unit is older. Other than this one local relationship, it is not possible to determine which unit is the oldest in this quadrangle.

This earlier period represented by units t, pdA, pfA, and plmA was followed by the formation of the most extensive unit in this quadrangle, unit pcA. These composite plains also have an unknown emplacement time. They were emplaced in a patchwork-style fashion, unlike more sheetlike extensive plains units seen in other regions of Venus (for example, Crown and others, 1994). Sources for the flows that make up these plains include small edifices, larger volcanoes, caldera complexes, and coronae.

Concurrent with and following the emplacement of unit pcA were episodes of volcanism (both edifice-forming and plains-forming), corona formation, wrinkle ridge formation, rifting, and extensional faulting. These events appear to overlap in time and space in the Aino Planitia region. For example, intense deformation is exhibited both in older patches of tessera and in the interiors of younger coronae. Rifts both predate and postdate plains-forming units.

Coronae in this area range from simple to complex, with features such as Ohogetsu and Copia Coronae sites of long-term geologic activity. Copia Corona, in particular, has undergone multiple episodes of volcanism and annulus formation. For example, some flows of Copia are cut by wrinkle ridges and others are not, and Indrani Corona formed between Copia volcanic episodes. Khotun and Cailleach flows formed after Makh Corona flows (unit fMk). The youngest Aramaiti Corona flows (units fA_a) superpose unit D of the Ohogetsu Corona flow material (unit fO_d). However, most of the coronae in this region are not in contact. Only Nishtigri Corona clearly predates unit pcA formation, although other coronae may have begun forming before unit pcA emplacement.

Kunapipi Mons, Mezrina Patera, and most small edifices formed after or during the formation of unit pcA. Evidence for earlier volcanism is seen in plains units plmA and pfA, which are interpreted to be volcanic materials, and in older small edifices in unit plmA. These older plains units suggest that the style of volcanism has not changed over time.

The most recent activity in the quadrangle has been edifice-forming volcanism (for example, Kunapipi Mons and unit e) and corona-related volcanism (for example, unit fCp_c). The earliest flows of Copia Corona (unit fCp_a) predate older flows from Kunapipi Mons (unit fK_2), as do flows from Ohogetsu Corona (unit fO_a predates unit fK_2). However, later flows from Ohogetsu cover Kunapipi Mons flows (unit fO_c postdates unit fK_2). The complexities seen at Kunapipi Mons are similar to those seen at terrestrial volcanoes, but as with coronae, determining the onset of activity is not possible, with early volcano or corona units possibly interbedded with plains units (Guest and Stofan, 1999).

Crater counts for Venus indicate that the overall surface has an average crater retention age of about 750 m.y. (McKinnon and others, 1997). The geologic activity in the Aino region during this period has consisted of multiple episodes of plains-forming volcanism, minor regional deformation in the form of extensional fractures and wrinkle ridges, corona formation, rifting associated dominantly with Juno Chasma, and edifice-forming volcanism. Most of these events appear to overlap in time; we find no support for the directional global stratigraphy proposed by Basilevsky and Head (1995).

REFERENCES

Anderson, S.W., Stofan, E.R., Plaut, J.J., and Crown, D.A., 1998, Block size distributions on silicic lava flow surfaces—Implications for emplacement conditions: Geological Society of America Bulletin, v. 110, p. 1258–1267.

Basilevsky, A.T., and Head, J.W., 1995, Global stratigraphy of Venus—Analysis of a random sample of thirty-six test areas: Earth, Moon, and Planets, v. 66, no. 3, p. 285–336.

Bridges, N.T., 1997, Ambient effects on basalt and rhyolite lavas under venusian, subaerial, and subaqueous conditions: Journal of Geophysical Research, v. 102, p. 9243–9255.

Bridges, N.T., and Fink, J.H., 1992, Aspect rations of lava domes on the Earth, Moon and Venus, *in* Abstracts of the 23d Lunar and Planetary Science Conference: Houston, Lunar and Planetary Institute, p. 159–160.

Campbell, B.A., 1999, Surface formation rates and impact crater densities on Venus: Journal of Geophysical Research, v. 104, no. E9, p. 21,951–21,956.

Campbell, B.A., and Campbell, D.B., 1992, Analysis of volcanic surface morphology on Venus from comparison of Arecibo, Magellan, and terrestrial airborne radar data: Journal of Geophysical Research, v. 97, no. E10, p. 16,293–16,314.

Copp, D.L., Guest, J.E., and Stofan, E.R., 1998, New insights into coronae evolution—Mapping on Venus: Journal of Geophysical Research, v. 103, no. E8, p. 19,401–19,418.

Crown, D.A., Stofan, E.R., and Plaut, J.J., 1994, Geology of the Guinevere Planitia quadrangle of Venus, *in* Abstracts of the 25th Lunar and Planetary Science Conference: Houston, Lunar and Planetary Institute, p. 301–302.

Fink, J.H., and Griffiths, R.W., 1990, Radial spreading of viscous-gravity currents with solidifying crust: Journal of Fluid Mechanics, v. 221, p. 485–509.

Ford, P.G., and Pettengill, G.H., 1992, Venus topography and kilometer-scale slopes: Journal of Geophysical Research, v. 97, no. E8, p. 13,103–13,114.

Ford, J.P., Plaut, J.J., Weitz, C.M., Farr, T.G., Senske, D.A., Stofan, E.R., Michaels, Gregory, and Parker, T.J., 1993, Guide to Magellan image interpretation: Jet Propulsion Laboratory Publication 93-24, 148 p.

Guest, J.E., 1983, Styles of eruption and flow morphology on Mt. Etna, *in* Romano, Romolo, ed., Mount Etna Volcano—A Review of Recent Earth Sciences Studies: Memorie della Società Geologica Italiana, v. XXIII—1982, p. 49–73.

Guest, J.E., Bulmer, M.H., Aubele, J.C., Beratan, Kathi, Greeley, Ronald, Head, J.W., Michaels, Gregory, Weitz, Catherine, and Wiles, Charles, 1992, Small volcanic edifices and volcanism in the plains of Venus: Journal of Geophysical Research, v. 97, p. 15,949–15,966.

Guest, J.E., Lancaster, M.G., Copp, D.L., and Stofan, E.R., 1996, Emplacement mechanisms for great lava flows on the plains of Venus—Slow vs. fast [abs.], *in* Whitehead, P.W., ed., Chapman Conference on Long Lava Flows, July 12–20, 1996, James Cook University, Townsville, Queensland, Australia: Economic Geology Research Unit Contribution, v. 56, p. 16–17.

Guest, J.E., and Stofan, E.R., 1997, Volcanic processes at large igneous provinces on Venus [abs.], *in* Volcanic Activity and the Environment, Abstracts of the IAVCEI General Assembly, Puerto Vallarta, Mexico, January 19–24, 1997: Guadalajara, Mexico, Unidad Editorial, p. 30.

———1999, A new view of the stratigraphic history of Venus: Icarus, v. 139, p. 55–66.

Hansen, V.L., and Willis, J.J., 1996, Structural analysis of a sampling of tesserae—Implications for Venus geodynamics: Icarus, v. 123, p. 296–312.

Hauck, S.A., Phillips, R.J., and Price, M.H., 1998, Venus—Crater distribution and plains resurfacing models: Journal of Geophysical Research, v. 103, no. E6, p. 13,635–13,642.

Head, J.W., Crumpler, L.S., Aubele, J.C., Guest, J.E., and Saunders, R.S., 1992, Venus volcanism—Classification of volcanic features and structures, associations, and global distribution from Magellan data: Journal of Geophysical Research, v. 97, no. E8, p. 13,153–13,197.

Ivanov, M.A. and Head, J.W., 1996, Tessera terrain on Venus—A survey of the global distribution, characteristics, and relation to surrounding units from Magellan data: Journal of Geophysical Research, v. 101, no. E6, p. 14, 861–14,908.

McGill, G.E., 1993, Wrinkle ridges, stress domains, and kinematics of venusian plains: Geophysical Research Letters, v. 20, no. 21, p. 2407–2410.

———1998, Central Eistla Regio—Origin and relative age of topographic rise: Journal of Geophysical Research, v. 103, p. 5889.

McGovern, P.J., and Solomon, S.C., 1997, Filling of flexural moats around large volcanoes on Venus—Implications for volcano structure and global magmatic flux: Journal of Geophysical Research, v. 102, no. E7, p. 16,303–16,318.

McKenzie, Dan, Ford, P.G., Liu, Fang, and Pettengill, G.H., 1992, Pancakelike domes on Venus: Journal of Geophysical Research, v. 97, no. E10, p. 15,967–15,976.

McKinnon, W.B., Zahnle, K.J., Ivanov, B.A., and Melosh, H.J., 1997, Cratering on Venus—Models and observations, *in* Brougher, S.W., Hunten, D.M., and Phillips, R.J., eds., Venus II: Tucson, University of Arizona Press, 1362 p.

Pavri, Betina, Head, J.W., Klose, K.B., and Wilson, Lionel, 1992, Steep-sided domes on Venus—Characteristics, geologic setting, and eruption conditions from Magellan data: Journal of Geophysical Research, v. 97, no. E8, p. 13,445–13,478.

Pettengill, G.H., Ford, P.G., and Wilt, R.J., 1992, Venus surface radiothermal emission as observed by Magellan: Journal of Geophysical Research, v. 97, no. E8, p. 13,091–13,102.

Phillips, R.J., Arvidson, R.E., Boyce, J.M., Campbell, D.B., Guest, J.E., Schaber, G.G., and Soderblom, L.A., 1991, Impact craters on Venus—Initial analysis from Magellan: Science, v. 252, p. 288–297.

Plaut, J.J., Stofan, E.R., Crown, D.A., and Anderson, S.W., 1994, Topographic and surface roughness properties of steep-sided domes on Venus and Earth from radar remote sensing and field measurements, *in* Abstracts of the 25th Lunar and Planetary Science Conference: Houston, Lunar and Planetary Institute, p. 1091–1092.

Plescia, J.B., and Golombek, M.P., 1986, Origin of planetary wrinkle ridges based on study of terrestrial analogs: Geological Society of America Bulletin, v. 97, p. 1289–1299.

Sakimoto, S.E.H., and Zuber, M.T., 1995, The spreading of variable-viscosity axisymmetric radial gravity currents—Applications to the emplacement of venusian 'pancake' domes: Journal of Fluid Mechanics, v. 301, p. 65–77.

Schaber, G.G., Strom, R.G., Moore, H.J., Soderblom, L.A., Kirk, R.L., Chadwick, D.J., Dawson, D.D., Gaddis, L.R., Boyce J.M., and Russell, Joel, 1992, Geology and distribution of impact craters on Venus—What are they telling us?: Journal of Geophysical Research, v. 97, no. E10, p. 13,257–13,302.

Smrekar, S.E., and Stofan, E.R., 1997, Coupled upwelling and delamination—A new mechanism for coronae formation and heat loss on Venus: Science, v. 277, p. 1289–1294.

———1999, Origin of corona-dominated topographic rises on Venus: Icarus, v. 139, p. 100–115.

Squyres, S.W., Jankowski, D.G., Simons, Mark, Solomon, S.C., Hager, B.H., and McGill, G.E., 1992, Plains tectonism on Venus—The deformation belts of Lavinia Planitia: Journal of Geophysical Research 97, 13,579–13,599.

Stofan, E.R., Anderson, S.W., Crown, D.A., Plaut, J.J., 2000, Emplacement and composition of steep-sided domes on Venus: Journal of Geophysical Research, v. 105, no. E11, p. 26,757–26,772.

Stofan, E.R., Bindschadler, D.L., Head, J.W., and Parmentier, E.M., 1991, Corona structures on Venus—Models of origin: Journal of Geophysical Research, v. 96, p. 20,933–20,946.

Stofan, E.R., and Guest, J.E., 1996, Geology of the Aino Planitia quadrangle (V–46)—Relative timing of tectonism and volcanism, *in* Abstracts of the 27th Lunar and Planetary Science Conference: Houston, Lunar and Planetary Institute, p. 1277–1278.

Stofan, E.R., Guest, J.E., and Copp, D.L., 2001, Development of large volcanoes on Venus—Constraints from Sif, Gula, and Kunapipi Montes: Icarus, v. 152, p. 75–95.

Stofan, E.R., Hamilton, V.E., Janes, D.M., and Smrekar, S.E., 1997, Coronae on Venus—Morphology and origin, *in* Brougher, S.W., Hunten, D.M., and Phillips, R.J., eds., Venus II: Tucson, University of Arizona Press, 1362 p.

Stofan, E.R., Head, J.W., Campbell, D.B., Zisk, S.H., Bogomolov, A.F., Rzhiga, O.N., Basilevsky, A.T., and Armand, N., 1989, Geology of a Venus rift zone—Beta Regio and Devana Chasma: Geological Society of America Bulletin, v. 101, p. 143–156.

Stofan, E.R., Smrekar, S.E., Bindschadler, D.L., and Senske, D.A., 1995, Large topographic rises on Venus—Implications for mantle upwelling: Journal of Geophysical Research, v. 100, no. E11, p. 23,317–23,328.

Wilhelms, D.E., 1972, Geologic mapping of the second planet: U.S. Geological Survey Interagency Report, Astrogeology 55.

———1990, Geologic mapping, *in* Greeley, Ronald, and Batson, R.M., eds., Planetary Mapping: New York, Cambridge University Press, p. 208–260.

Zahnle, K.J., 1992, Airburst origin of dark shadows on Venus: Journal of Geophysical Research, v. 97, no. E6, p. 10,243–10,255.

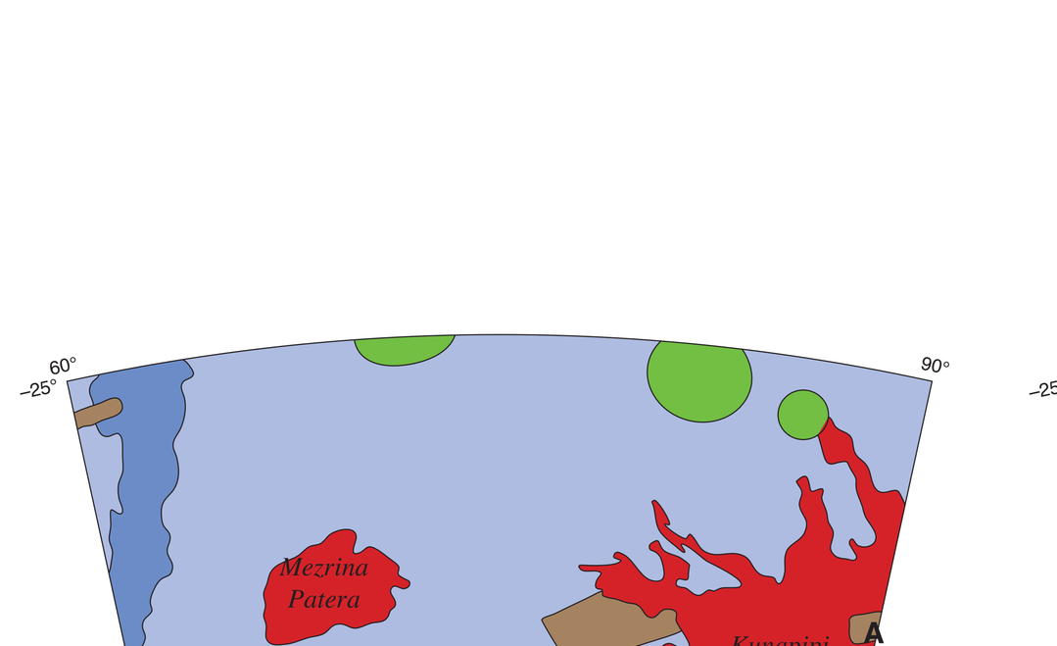

Figure 1. Geomorphologic map of V–46 quadrangle showing major features (volcanoes, coronae, rifts, a ridge belt, and a plateau). Copia Corona, Kunapipi Mons, Mezrina Patera, and Juno Chasma are also indicated. **A**, **B**, and **C** indicate sections of Juno Chasma; **P** indicates northern end of Lada Terra plateau.

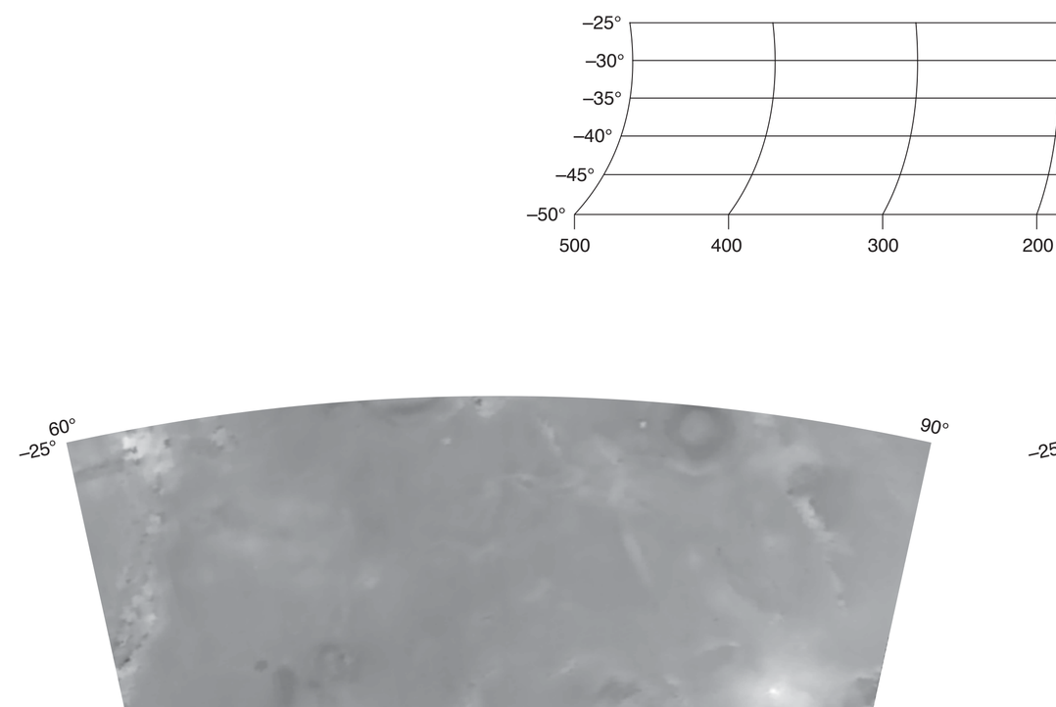

Figure 2. Topographic map of V–46 quadrangle from Magellan altimetry data. Topographic high at Kunapipi Mons is clearly visible, as is the raised central region and rims of Copia Corona.

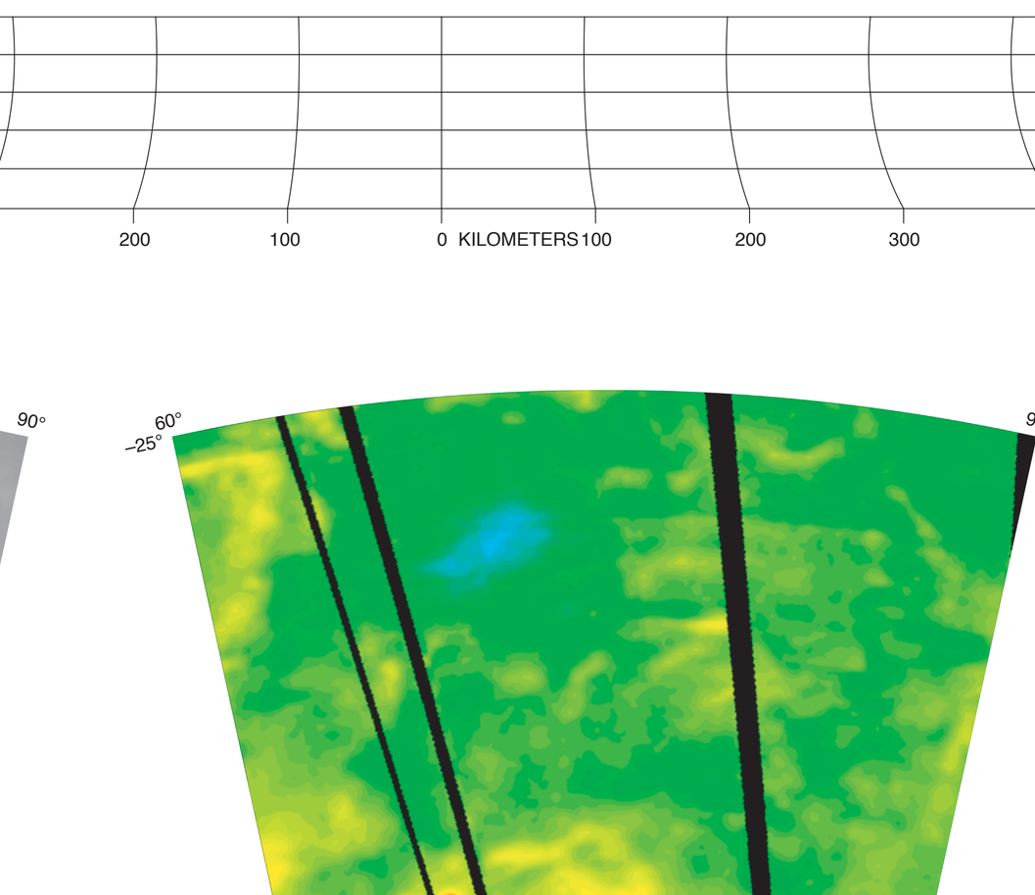

Figure 3. Magellan emissivity map of V–46 quadrangle. Much of the region has relatively uniform emissivity, with the exception of elevated values over rifts in the southwestern corner of the quadrangle.

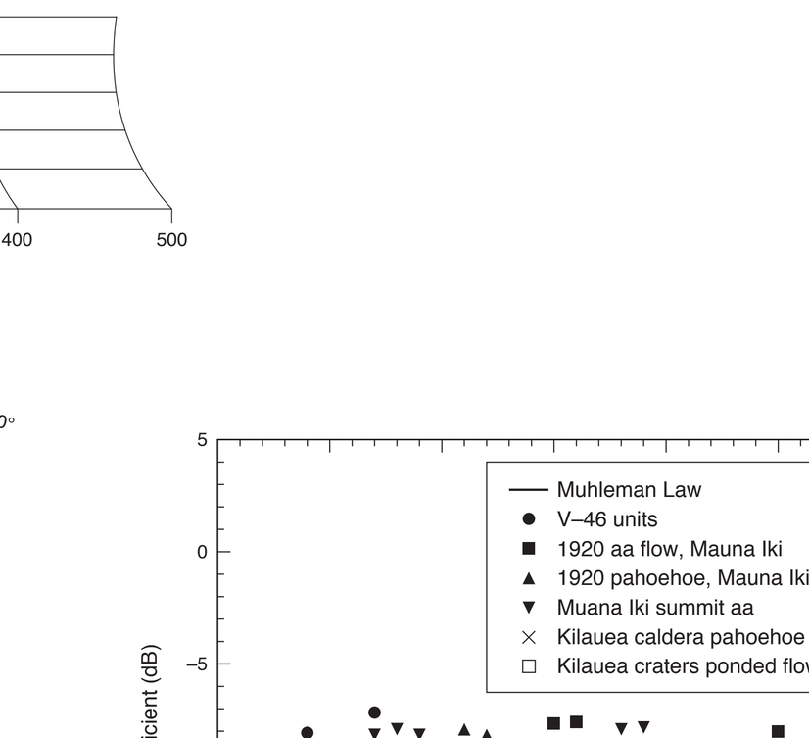

Figure 4. Plot showing relationship between incidence angle and backscatter coefficient for units in V–46 quadrangle. Synthetic aperture radar (SAR) echo values for this plot and for table 2 were derived using the mgn_data program; other values in table 2 were derived using anc_data program. Typical errors are about ±1 dB for these measurements (for example, Campbell and Campbell, 1992).

Table 1. *Coronae within V–46 quadrangle.*

Corona name	Location	Maximum width (km)
Aramaiti	26.3° S., 82° E.	350
Cailleach	48.0° S., 88.3° E.	125
Copia	42.5° S., 75.5° E.	500
Indrani	37.5° S., 70.5° E.	200
Khotun	46.5° S., 81.5° E.	200
Makh	48.7° S., 85.0° E.	200
Nishtigri	24.5° S., 72.0° E.	275
Ohogetsu	27.0° S., 85.7° E.	175

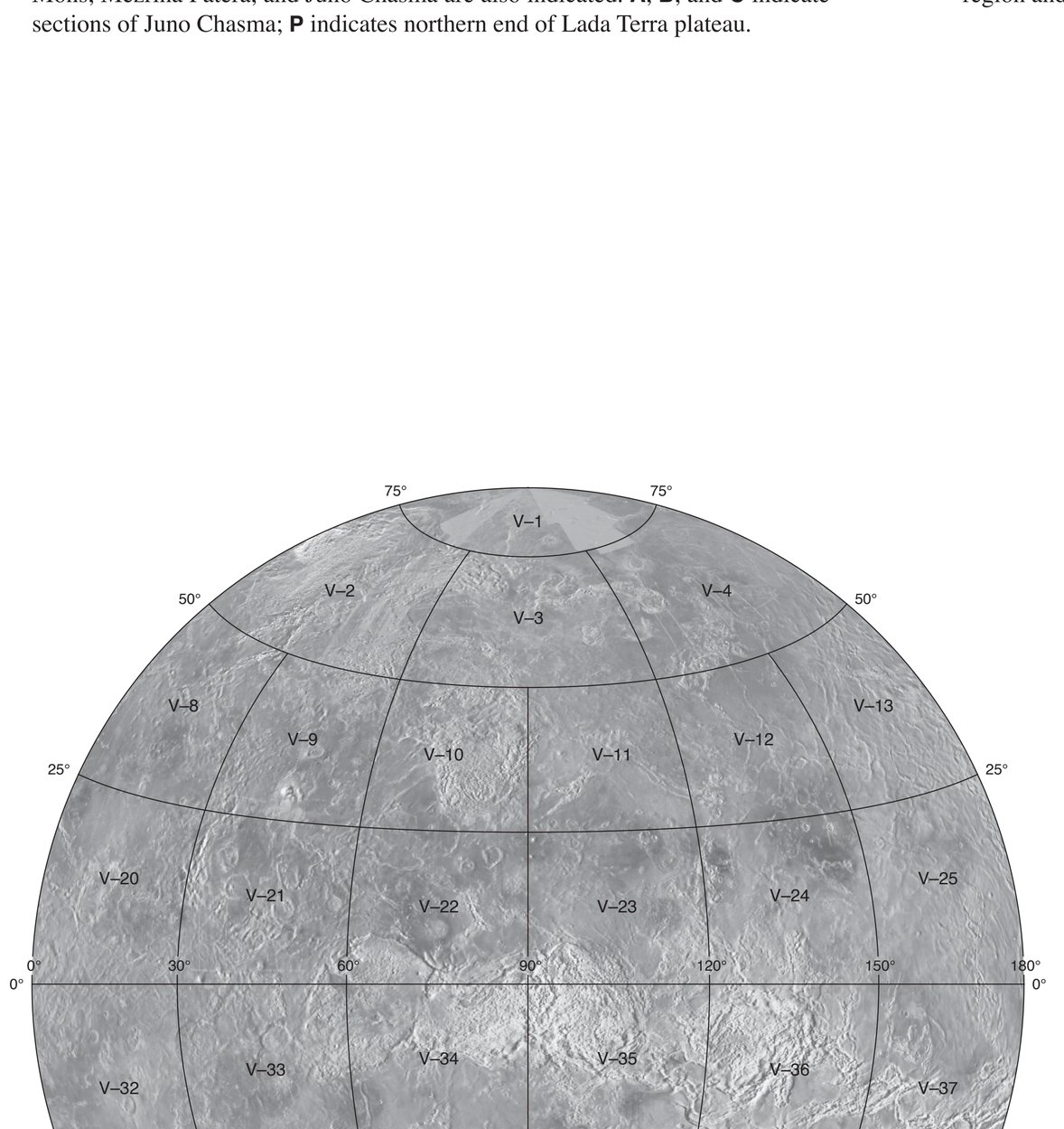

QUADRANGLE LOCATION
Photomosaic showing location of map area. An outline of 1:5,000,000-scale quadrangles is provided for reference.

Table 2. *Radar properties for units within V–46 quadrangle.*

Unit	Latitude	Longitude	Box size	Radius (km)			RMS Slope			Reflectivity			Emissivity			Inc. angle	Dielectric		Backscatter (dB)		
			(°)	Mean	Min	Max	Mean	Min	Max	Mean	Min	Max	Mean	Min	Max	(°)	Smooth	Rough	Mean	Min	Max
pdA_b	–30	62	0.5	6051.65	6051.04	6052.134	3.91	2.5	6.9	0.087	0.065	0.11	0.873	0.863	0.882	33	3.4	4.4	–9.64	–18.69	3.86
pfA	–31	70	0.2	6051.384	6051.314	6051.566	2.55	2.3	3.3	0.138	0.13	0.145	0.821	0.82	0.822	33	4.6	6	–12.77	–17.71	–2.3
plmA	–46	74	0.5	6052.012	6051.834	6052.278	3.51	2.1	5.3	0.079	0.065	0.11	0.868	0.865	0.872	25	3.9	4.6	–9.48	–14.76	1.08
pcA	–31	66	0.5	6051.187	6051.14	6051.227	2.8	2.2	3.5	0.12	0.11	0.135	0.846	0.838	0.852	33	4	5.2	–14.53	–19.14	1.08
puA	–46.5	89	0.5	6051.255	6051.173	6051.302	2.63	1.8	3.5	0.085	0.065	0.105	0.881	0.877	0.884	25	3.7	4.2	–10.88	–15.42	–4.36
psA	–43.5	89.5	0.2	6051.042	6051.022	6051.063	2.1	1.6	2.5	0.106	0.095	0.12	0.861	0.86	0.862	26	4.1	4.8	–11.94	–15.69	–6.5
pN	–25.2	69.75	0.2	6050.734	6050.552	6050.933	2.93	1.7	4.3	0.087	0.075	0.11	0.868	0.865	0.869	36	3.3	4.5	–12.42	–18.7	–2.68
fMk	–49.25	86.5	0.2	6051.301	6051.27	6051.327	3.01	2.6	3.3	0.103	0.095	0.12	0.878	0.877	0.879	24	3.8	4.3	–9.5	–12.74	–5.96
pMk	–48	84.5	0.5	6051.191	6050.622	6051.393	4.35	3.2	6.9	0.073	0.055	0.135	0.904	0.899	0.909	24	3.2	3.6	–8.14	–14.02	–2.82
fCl_1	–47.1	88	0.2	6051.131	6051.086	6051.171	2.48	1.8	2.9	0.069	0.06	0.08	0.883	0.881	0.884	25	3.6	4.2	–10.64	–14.71	–4.71
fCl_2	–48.75	88	0.2	6051.226	6051.138	6051.332	2.93	2.5	3.8	0.079	0.075	0.09	0.889	0.887	0.89	24	3.5	4	–9.14	–12.85	–4.83
fCp_a	–39.15	70	0.5	6051.56	6051.506	6051.63	2.68	2.3	3.3	0.101	0.08	0.115	0.859	0.855	0.861	28	4	4.8	–11.26	–16.16	–4.81
fMr_1	–46	70	0.5	6051.769	6051.75	6051.818	3.25	2.7	4	0.111	0.1	0.14	0.855	0.852	0.859	25	4.3	4.9	–10.24	–13.79	–5.96
fMr_2	–48.5	70	0.5	6052.076	6051.889	6052.232	2.93	1.9	4.2	0.101	0.085	0.12	0.859	0.854	0.863	24	4.2	4.8	–8.92	–13.55	–1.9
fI	–37.75	69.3	0.2	6051.198	6051.146	6051.281	2.34	2	2.9	0.1	0.09	0.115	0.856	0.855	0.857	29	4	4.9	–13.4	–17.46	–8.06
pI	–37.25	70.2	0.2	6051.592	6051.529	6051.698	3.64	3	4.1	0.101	0.085	0.125	0.864	0.862	0.865	29	3.8	4.7	–12.25	–17.14	–5.93
fKh	–48	80	0.5	6051.215	6051.125	6051.275	4.07	3.3	4.7	0.101	0.085	0.12	0.879	0.876	0.882	24	3.7	4.3	–9.25	–12.76	–4.4
fO_a	–27	86	0.2	6051.177	6051.018	6051.315	2.94	2.1	3.5	0.153	0.14	0.18	0.841	0.839	0.843	35	4	5.3	–15.57	–21.18	–4.95
fO_b	–26.9	86.5	0.2	6051.049	6050.983	6051.13	2.59	1.8	4.1	0.141	0.12	0.19	0.842	0.84	0.845	35	3.9	5.3	–14.75	–20.36	–2.39
fO_c	–26.6	84.8	0.2	6051.849	6051.79	6051.919	2.2	1.7	2.5	0.109	0.095	0.13	0.842	0.841	0.845	35	3.9	5.3	–15.88	–20.04	–9.63
fO_d	–27	85.9	0.5	6051.528	6051.314	6051.769	2.13	1.6	2.7	0.116	0.1	0.13	0.845	0.841	0.847	35	3.9	5.2	–15.08	–20.57	0.84
fCp_c	–41.5	77.5	0.5	6051.562	6051.35	6051.842	3.95	2.7	5.7	0.073	0.035	0.11	0.883	0.874	0.892	27	3.5	4.1	–10.93	–15.93	–2.12
fCp_d	–42.2	69.5	0.5	6051.102	6051.035	6051.165	2.07	1.2	2.8	0.093	0.075	0.11	0.867	0.863	0.874	27	3.9	4.6	–11.53	–14.08	–5.28
fCp_f	–41.5	72	0.5	6051.684	6051.57	6051.825	2.92	1.9	4.3	0.069	0.055	0.085	0.876	0.87	0.878	27	3.7	4.3	–10.48	–16.32	–2.92
fCp_b	–43	79.5	0.5	6051.048	6051.001	6051.111	2.67	1.9	3.5	0.089	0.08	0.1	0.871	0.868	0.875	27	3.8	4.5	–10.34	–13.87	–6.61
fA_a	–26.85	83.6	0.2	6051.338	6051.227	6051.442	2.24	1.6	2.5	0.116	0.105	0.13	0.852	0.848	0.857	35	3.7	5	–11.88	–14	–7.4
fA_b	–25.15	82	0.2	6050.274	6050.162	6050.437	2.33	1.7	2.7	0.132	0.115	0.145	0.842	0.841	0.844	36	3.9	5.3	–16.33	–21.26	–7.48
fA_c	–26	83.1	0.2	6050.889	6050.825	6050.95	2.78	2.4	3.5	0.135	0.11	0.145	0.847	0.843	0.851	35	3.8	5.1	–14.38	–20.14	–6.71
fA_e	–25.9	79.2	0.5	6051.066	6050.996	6051.173	1.58	1	2.7	0.1	0.08	0.13	0	****	0	35	0	0	–11.44	–14	–9.59
fK_3	–32.75	79.5	0.5	6051.305	6051.251	6051.361	2.9	1.7	5.6	0.089	0.075	0.115	0.881	0.865	0.893	32	3.3	4.2	–10.18	–17.71	–5.2
fK_1	–30.3	88.5	0.2	6051.606	6051.57	6051.634	2.17	2	2.7	0.124	0.12	0.13	0.859	0.858	0.861	33	3.7	4.8	–15.01	–21.38	–10.4
fK_2	–39	89	0.2	6050.98	6050.96	6050.999	1.83	1.3	2.6	0.095	0.085	0.105	0.861	0.86	0.863	28	3.9	4.8	–14.24	–18.59	–7.78
fMe	–34	69.5	0.2	6050.781	6050.696	6050.874	2.23	1.8	2.7	0.079	0.07	0.09	0.856	0.854	0.859	31	3.9	4.9	–13.52	–17.16	–8.36
fK_3	–33.5	84.1	0.5	6051.827	6051.455	6052.094	2.65	1.8	3.9	0.122	0.105	0.16	0.858	0.854	0.862	31	3.8	4.8	–14.63	–19.6	–9.39
sK_1	–33.8	87.2	0.2	6052.814	6052.525	6053.056	3.76	2.8	4.9	0.12	0.095	0.14	0.859	0.855	0.863	31	3.8	4.8	–10.37	–19.14	0.66
sK_2	–33.75	86.1	0.2	6053.374	6053.043	6054.136	3.7	2.8	5.3	0.1	0.07	0.185	0.845	0.843	0.847	31	4.1	5.2	–11.03	–19.13	2.63
d	–25.9	80	0.2	6051.509	6051.462	6051.548	1.82	1.5	2.1	0.133	0.115	0.155	0	****	0	35	0	0	–13.2	–15.39	–5.79
f	–29.2	88	0.2	6051.335	6051.272	6051.398	2.29	2.1	2.7	0.134	0.115	0.155	0.836	0.835	0.838	34	4.1	5.5	–13.58	–15.81	–11.01
e	–30.7	68.5	0.2	6051.295	6051.252	6051.332	2.49	2.1	2.8	0.132	0.12	0.145	0.833	0.832	0.834	33	4.3	5.6	–16.23	–20.16	–9.57
t	–25.2	65.25	0.2	6051.517	6051.398	6051.617	5.42	2.8	7.6	0.09	0.055	0.18	0.884	0.881	0.888	36	3	4	–9.86	–17.3	–1.1
c	–37.99	63.68	0.2	6050.648	6050.579	6050.832	1.02	0.3	2.2	0.073	0.06	0.085	0.881	0.878	0.884	29	3.5	4.2	–10.83	–17.26	2.54

Table 3. *Craters within V–46 quadrangle.*

Crater name	Location	Diameter (km)	Superposed on	Superposed by
Agrippina	33.2° S., 65.7° E.	38.6	fMe, pcA	
Emilia	26.5° S., 88.2° E.	12.5	pcA	
Germain	37.9° S., 63.7° E.	35.5	fCp_a, pcA	
Jodi	35.7° S., 68.7° E.	10.2	pcA	
Leila	44.2° S., 86.8° E.	18.8	pcA	puA
Mansa	33.9° S., 63.4° E.	8.1	pcA	
Maurea	39.5° S., 69.1° E.	9.9	fCp_a	
Raki	49.4° S., 70.0° E.	7.5	fMr_2	
Ruit	25.5° S., 72.9° E.	6.4	d, pcA	
Samintang	39.0° S., 88.7° E.	25.9	fCp_a	
Shushan	43.8° S., 70.2° E.	8.5	fCp_a	
Tehina	30.4° S., 76.4° E.	5.4	pcA	
Teumere	38.3° S., 88.1° E.	5.4	fCp_a	
Francesca (V–45/V–46)	28.0° S., 57.7° E.	17	pcA	

GEOLOGIC MAP OF THE AINO PLANITIA QUADRANGLE (V–46), VENUS

By
Ellen R. Stofan and John E. Guest
2003

For sale by U.S. Geological Survey, Information Services, Box 25286, Federal Center, Denver, CO 80225, 1–888–ASK–USGS
Digital files available on World Wide Web at http://pubs.usgs.gov/imap/i2779
ISBN 0-607-89377-X
9 780607 893779
Printed on recycled paper